Res Chem Intermed (2015) 41:1893–1906
DOI 10.1007/s11164-013-1318-6

Study on the dehydration kinetics of tunellite using non-isothermal methods

Müge Sari Yilmaz · Aysel Kantürk Figen · Sabriye Pişkin

Received: 23 January 2013 / Accepted: 14 June 2013 / Published online: 28 June 2013
© Springer Science+Business Media Dordrecht 2013

Abstract The thermal behavior of tunellite has been examined by using thermal analysis data at different heating rates. Coats–Redfern, Horowitz–Metzger, Piloyan–Novikova, Doyle, and isoconversional Ozawa kinetic models have been used for the non-isothermal dehydration kinetic investigation of the mineral. The kinetic parameters are computed using the above-mentioned models for all dehydration stages. In addition, structural characterizations of tunellite are analyzed by using an X-ray diffractometer, an inductive coupled plasma-optical emission spectroscopy, Fourier transform infrared spectroscopy, and a scanning electron microscope.

Keywords Tunellite · Dehydration · Kinetic analysis · Isoconversional methods · Piloyan novikova

Introduction

Turkey has rich boron resources (883 million tons B_2O_3), comprising approximately 67 % of the world's known boron reserves. These boron reserves are high in tenor and quality [1]. The substantial boron reserves in Turkey are generally located in the districts of Bigadic, Balikesir, Kirka, and Kestelek [2].

Different from the other known boron reserves in Turkey, the Kirka borate deposits mainly contain Na-borate and Na, Ca, Mg, Ca, and Mg–Ca, and Sr-borate minerals [3]. Tunellite ($SrB_6O_9(OH)_2{\cdot}3H_2O$) and veachite ($Sr_2B_{11}O_{16}(OH)_5{\cdot}H_2O$) are the commonly known types of Sr-borate minerals. Generally, these two minerals occur together and their compositions are similar, but they have different lattice structures. Tunellite, which is a dehydrated strontium borate, shows a monoclinic

M. Sari Yilmaz · A. Kantürk Figen · S. Pişkin (✉)
Department of Chemical Engineering, Yildiz Technical University, Topkapi, Istanbul, Turkey
e-mail: piskin@yildiz.edu.tr

structure similar to most boron minerals and is also found in association with ulexite and colemanite [4].

Many theoretical methods for kinetic analysis have been reported in the literature. These methods help to understand the following reaction type: solid → solid + gas. The kinetics of thermal decompositon of the lanthanum (III) complex for the second stage was studied by the Achar differential method and the Coats–Redfern integral method [5]. Park et al. [6] developed a kinetic analysis method by using a dynamic model that can account for the thermal decomposition behavior of polymers with the variation of the conversion. The thermal dehydration kinetics of titanate nanotubes were investigated by the Vyazovkin model-free kinetic method [7]. The dehydroxylation kinetic parameters of naturally occurring sepiolite and bentonite were determined by the Flynn–Wall–Ozawa, Kissenger–Akahira–Sunose, and Friedman isoconversional methods [8].

In the production of boron compounds, dehydration of the boron minerals, which have been investigated mostly with thermogravimetric methods, has a great importance. Decomposition kinetics of boron minerals and compounds have been investigated for many years. Piskin examined the thermal properties of tincalconite, borax, kernite, probertite, ulexite, colemanite, hydroboracite, meyerhofferite, inyonite, kurnakovite, inderite, tunellite, howlite, and veacite hydrate boron minerals. In addition, the chemical and structural properties of these minerals were also examined by IR spectrometry and XRD analysis [9]. Ekmekyapar et al. [10] determined the dehydration kinetics of tincal and borax minerals by TG and DTA analysis. The activation energies, frequency factor, and order of reaction for both minerals were calculated by using various kinetic methods. Sevim et al., determined the kinetic parameters of thermal decomposition of boric acid by using the Coats–Redfern and Suzuki methods. The Coats–Redfern method was proved to generate better results compared to the Suzuki method because of its applicability to both regions separately [11].

Şener et al. [12] examined the thermal reactions of ulexite by using TG, DTG, and DTA techniques. The decomposition of ulexite mineral occurred with two stages of dehydration followed by two stages of dehydroxylation in the temperature range 60–500 °C. Okur and Eymir analyzed the calcination kinetics of ulexite by applying the Coats–Redfern and genetic algorithm methods on TG. They proved that, for the low activation energy reactions, the Coats–Redfern method could not be applied [13]. By using the Coats–Redfern method, Kanturk et al. [14] determined the kinetic analysis of sodium metaborate hydrate used in sodium borohydride ($NaBH_4$) production as a starting material. Kinetic parameters (E and k_0) were computed by assuming first-order reactions. The dehydration kinetics of inderite was investigated by different non-isothermal kinetic methods [15]. The Ozawa, Kissenger, and Doyle methods were performed in the stage of decomposition of admontite magnesium borate mineral [16].

Dehydration of the hydrated boron minerals have become significant issues in the production of boron compounds. Although there have been many investigations of dehydration kinetics of different boron minerals, there are few studies on the dehydration kinetics of tunellite in the literature. The decomposition kinetics of tunellite was studied by using the Arrhenious equation. In these analyses, the order

of the dehydration reaction was assumed to be first-order, and the activation energy, pre-exponential factor, and rate constant were calculated [17]. The effect of heat treatment on the structural characteristics and dehydroxylation kinetics of the tunellite was investigated in our previous study [18].

In the present study, non-isothermal kinetic parameters of dehydration at different heating rates were examined by using the Coats–Redfern (C–R), Horowitz Metzger (H–M), Piloyan-Novikova (P–N), Doyle (DY), and isoconversional Ozawa (OW) kinetic models. The dehydration of tunellite takes place in three stages and the kinetic parameters (activation energies, pre-exponential factors, rate constants, and reaction orders) were computed for each dehydration stage. In addition, tunellite was characterized using X-ray diffractometer (XRD), inductive coupled plasma–optical emission spectroscopy (ICP-OES), Fourier transform infrared spectroscopy (FT-IR), and scanning electron microscope (SEM) analysis techniques to identify its structural properties.

Experimental

Materials and characterization

The tunellite used in the study was provided from the region of Kirka, Eskisehir, in Turkey. After manually cleaning the mineral of visible impurities, it was ground and sieved to give a particle size of 250 mesh by an ASTM standard sieve. The chemical analysis of tunellite was found to be B_2O_3 54.19 % and SrO 27.02 % from ICP-OES, and the total average weight loss was 18.59 % calculated at 36–718 °C from TG/DTG analysis.

X-ray analysis of mineral was investigated by XRD on a Philips Panalytical X'Pert Pro instrument with CuKα radiation at operating parameters of 40 mA and 45 kV. Data were recorded at room temperature with a diffraction angle from 10° to 70°; phase identification of the mineral was performed by International Centre for Diffraction Data (ICDD) database that is available on X'Pert High Score Plus software of the XRD equipment. The XRD pattern of tunellite is shown in Fig. 1.

Quantitative analysis of the trace elements within the mineral was performed by using the ICP-OES model Perkin Elmer, Optima 2100 DV, in which 0.1 g of mineral was digested in nitric, hydrofluoric, hydrochloric, and phosphoric acids, followed by dilution and analysis. The sample was analyzed more than two times and mean values were used as one observation.

The FT-IR spectrum was obtained in a model Perkin Elmer Spectrum One spectrometer, at the 4,000–450 cm^{-1} range (4 scans, resolution: 8 cm^{-1}). Before the FT-IR analysis, the sample was mixed with KBr powder at the ratio 1:100, and a pellet was made by applying a loading of 10 kg/cm^2 with a hydraulic press. The FT-IR spectrum is given in Fig. 2.

The morphologies of tunellite were observed by a JEOL (JSM-5610LV) SEM capable of producing high-resolution images of a sample surface; SEM images have a characteristic three-dimensional appearance (Fig. 3).

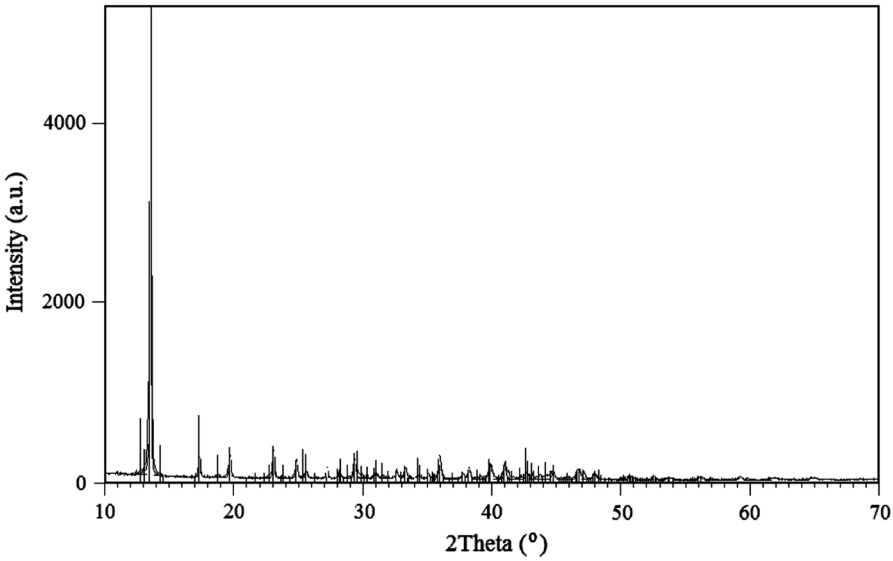

Fig. 1 XRD pattern of tunellite

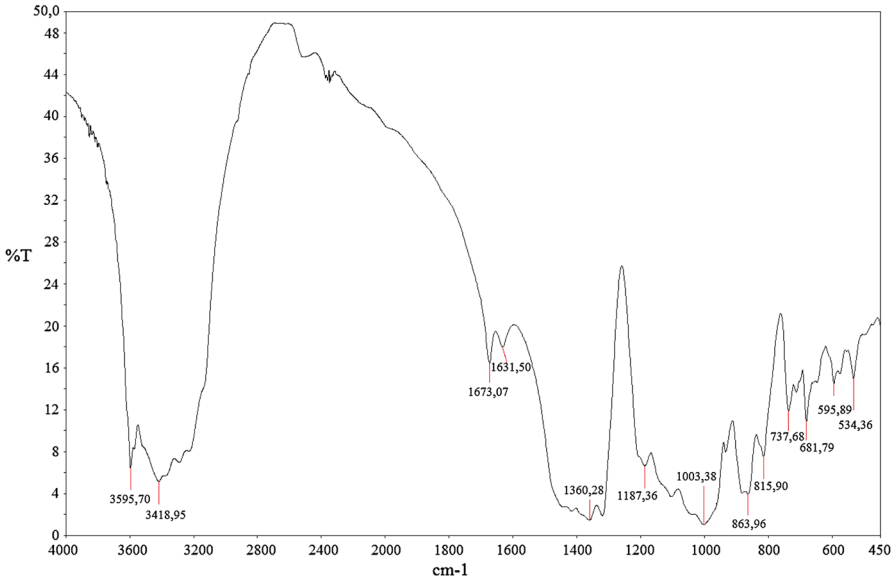

Fig. 2 FT-IR spectrum of tunellite

Thermal measurements

In this study, thermal analysis experiments were carried out with a Perkin Elmer Diamond TG\DTA instrument. This instrument was calibrated by means of the melting points of indium (156.6 °C) and tin (231.9 °C) as the standard substances

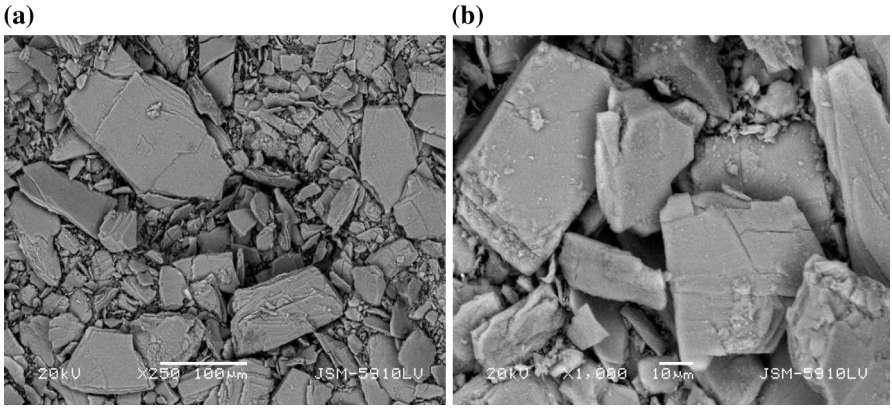

Fig. 3 SEM micrographs of tunellite **a** ×250, **b** ×1,000

under the same conditions as the sample. Approximately 13 mg of samples was put into a platinum crucible. The experiments were performed under different heating rates of 5, 10, 15, and 20 °C/min at the temperature range of 30–900 °C, and a 150 ml/min gas flow rate (pure nitrogen) was used.

Theoretical background of kinetic analysis

Recently, the interest in determining the rate-dependent parameters of solid-state non-isothermal decomposition reactions by analyzing TG/DTA curves has increased. In order to analyze TG/DTA curves and obtain values for kinetic parameters, many equations have been suggested [19–23].

In this study, the dehydration kinetics of tunellite were investigated by following non-isothermal methods, representative of different categories, and several equations were applied to the thermal data: C–R, H–M, P–N, DY, and isoconversional OW. The calculated kinetic parameters were reaction order (n), activation energy (E_a), and frequency factor (k_0).

The C–R equation is as follows:

$$\mathrm{In}\left[\frac{g(\alpha)}{T^2}\right] = \mathrm{In}\left[\frac{k_0 R}{\beta E_a}\left(1 - \frac{2RT}{E_a}\right)\right] - \frac{E_a}{RT} \quad (1)$$

where $g(\alpha) = \left[\frac{1-(1-\alpha)^{1-n}}{(1-n)}\right]$ $(n = 1,\ \mathrm{g}(\alpha) = -\mathrm{In}(1-\alpha)$, n is the reaction order, α is the degree of conversion, β is the heating rate, $(2RT/E_a) \cong 1$, k_0 is the pre-exponential factor, E_a is the activation energy, R is the gas constant, and T is the thermodynamic temperature. Plotting $\mathrm{In}[g(\alpha)/T^2]$ against $1/T$ at different n, E_a is calculated from the slope, and k_0 is determined from the intercept of the curve. When R (linear correlation coefficient) is at its largest, the corresponding n is the reaction order and its kinetic parameters (E_a and k_0) can be readily obtained [23].

Although C–R equations require detailed calculations, the calculations can be carried out only with the use of the TG curve. The net advantage of this method is the simultaneous determination of the reaction order and stages.

The H–M equation (Eq. 2) is illustrative of the approximation methods. In this method, ln[g(α)] is plotted with θ, and the resulting activation energy is calculated from the slope as follows:

$$\mathrm{In}[g(\alpha)] = \mathrm{In}\left(\frac{k_0 \cdot R \cdot T_s^2}{\beta.E_a}\right) - \frac{E_a}{R.T_s} + \frac{E_a.\theta}{RT_s^2} \qquad \text{for } n \neq 1 \tag{2}$$

where $g(\alpha) = \frac{1-(1-\alpha)^{1-n}}{1-n}$, the characteristic temperature is defined as $\theta = T - T_s$, and T_s is the DTG peak temperature [19].

In the P–N relationship (Eq. 3), the values of E_a and k_0 are obtained from the slope and intercept of the graph between $\log(\alpha/T^2)$ and 1/T by taking the values of α from 0.1 to 0.9 [20].

$$\log\left(\frac{\alpha}{T^2}\right) = \log\left(\frac{k_0 R}{\beta E_a}\right) - \left(\frac{E_a}{2.303RT}\right) \tag{3}$$

The DY method has a mathematically simplified equation and its use is easy. The DY equation is as follows:

$$-\log\beta = 0.4567\left(\frac{E_a}{RT_m}\right) + \text{Constant} \tag{4}$$

where T_m is the maximum peak temperature of the DTA curve. A plot of log β versus $1/T_m$ gives the $0.4567E_a/R$ slope for the most appropriate evaluation of the activation energy. In addition, k_0 can be calculated from the Eq. 5 [21].

$$k_0 = \exp\left(\frac{E_a}{RT_m}\right)\frac{\beta E_a}{RT_m} \tag{5}$$

For each degree of conversion, the logarithm of the heating rate, log β, against the inverse of the temperature was correlated according to the isoconversional OW method (Eq. 6). The E_a value is calculated from the slope of the log β ~ $1/T$ curve, which is equal to 0.4567(Ea/R) [22].

$$\log\beta = \log\left(\frac{k_0 E_a}{R}\right) - 2.315 - 0.4567\left(\frac{E_a}{RT}\right) - \log g(\alpha) \tag{6}$$

Despite the fact that the OW method presentd the advantage of not requiring previous knowledge of the reaction mechanism for determining the activation energy, the common disadvantage of this method is the requirement for several experiments with different heating rates.

Results and discussion

Structural characterization

The crystalline structure of the mineral was determined by the X-ray powder diffraction technique. The resulting diffractogram is given in Fig. 1. X-ray analysis of the mineral indicated that it was defined as tunellite with a chemical formula of $SrB_6O_9(OH)_2{\cdot}3H_2O$. In the sample, 6.53217 Å diffraction peak corresponding to a

Table 1 % composition and distribution of the trace elements

Element	Si	Mg	Ca	K	Ba	S	Al
(wt %)	0.19	0.0028	0.0025	0.002	0.001	0.0004	0.0004
Element	Cr	Fe	Cu	Ni	Zn	Pb	Na
(wt %)	0.0009	0.00007	0.00002	0.00001	0.00001	<0.00005	<0.00005

13.56° diffraction angle had the maximum intensity, which characterized tunellite in the monoclinic crystal system (PDF no: 01-074-1638).

The results of the ICP-OES quantitative analysis of trace elements in the mineral are shown in Table 1.

The FT-IR spectrum of tunellite exhibited the following absorption bands and they were assigned by referring to the literature [9]. The bands at 3,596 and 3,419 cm^{-1} are the stretching vibrations of the O–H group. The bands at 1,673 and 1,632 cm^{-1} are assigned to the H–O–H bending mode, showing that this mineral contains crystal water. Bands in the region 1,360 cm^{-1} are the asymmetric stretching mode of B(3)-O. The band at 1,187 cm^{-1} is assigned to the bending in-plane mode of O–H. The bands at 1,003, 864, and 816 cm^{-1} are the asymmetric and symmetric stretching modes of B(4)-O, respectively. The bands at 738, 682, 596, and 535 cm^{-1} are assigned to out-of-plane bending of B(3)-O (Fig. 2).

The SEM images of tunellite in Fig. 3 with different magnifications illustrate that the morphology of the crystallites was a plate-like structure.

Thermogravimetric analysis

TG and DTG thermograms of tunellite at different heating rates are given in Figs. 4 and 5. From the thermograms, it can be observed that thermal decomposition of tunellite occurred within the temperature range 36–718 °C with three dehydration stages followed by one dehydroxylation stage. The dehydration step of tunellite began at about 36 °C and continued up to 153 °C. Two partly overlapping peaks occurred at around 196 and 239 °C at 20 °C/min, which are shown in the DTG peaks. The dehydroxylation reaction, which corresponds to releasing of hydroxyl groups (OH^-) from the polyanion structure, proceeded up to 718 °C. The total weight losses of the dehydration and dehydroxylation reactions are calculated as 18.66 % for 20 °C/min heating rate. Weight losses of dehydration and dehydroxylation stages at different heating rates are given in Table 2.

The results of DTA analysis showed that there were four endothermic peaks (Fig. 6). The first three endothermic peaks that appear at 121, 177, and 222 °C, respectively, are due to the result of dehydration reactions at heating rate of 5 °C/min. For the other heating rates (10, 15, and 20 °C/min), these peak temperatures (T_m) are given in Table 3. The fourth endothermic peak corresponding to dehydroxylation reaction appeared at 447, 452, 456, and 458 °C for 5, 10, 15, and 20 °C/min heating rates, respectively. It is seen that the characteristic peak temperature increases as a function of the heating rates.

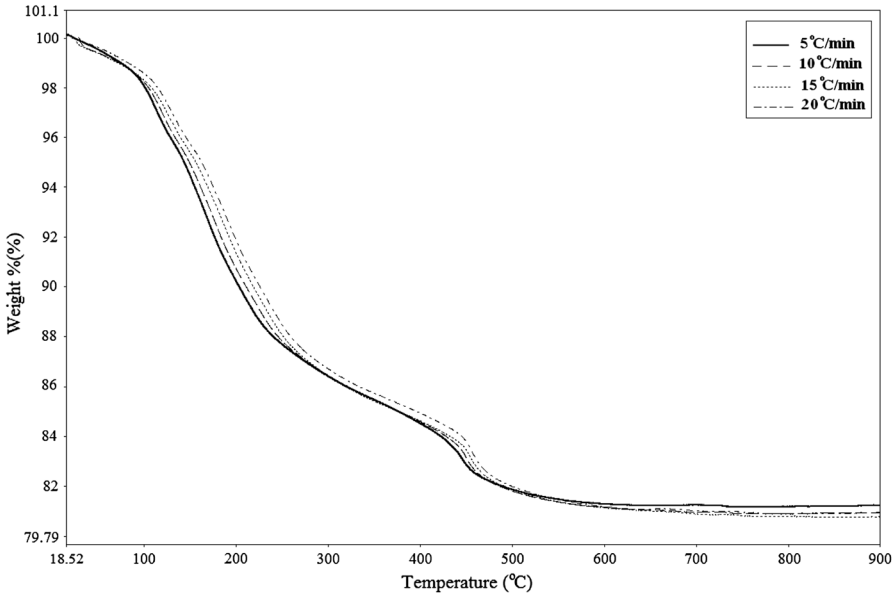

Fig. 4 TG thermograms of tunellite at different heating rates, N_2 flow rate 150 ml/min

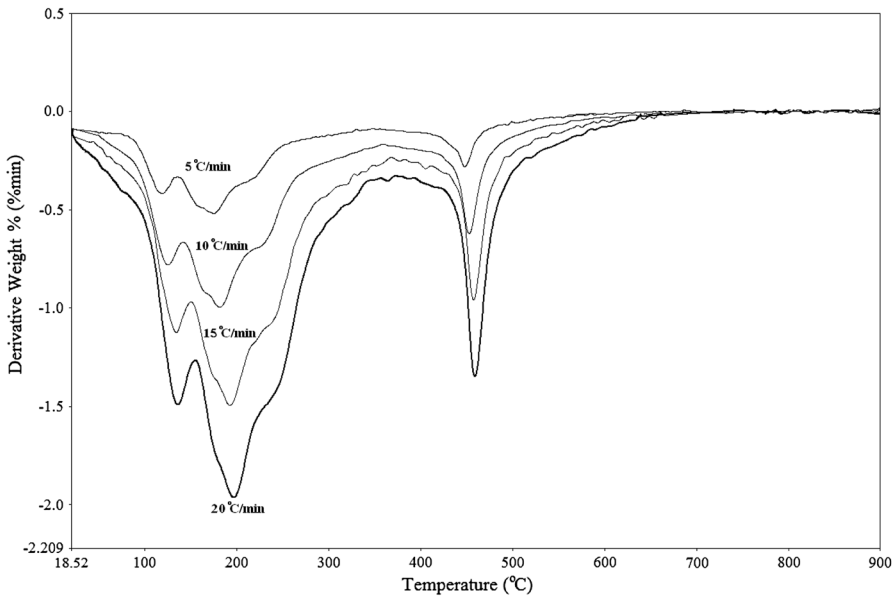

Fig. 5 DTG thermograms of tunellite at different heating rates

Kinetic analysis

In order to determine the dehydration kinetics of tunellite, we calculated the E_a with TG/DTA data in α range of 0.1–0.9 at the heating rates of 5, 10, 15, and 20 °C/min

Table 2 Weight losses of dehydration and dehydroxylation stages at different heating rates

β (°C/min)	Reaction steps	Temperature range(°C)	Weight loss (%)
5	Dehydration stages	I: 36.69–135.85	4.09
		II: 135.85–203.38	5.56
		III: 203.38–383.01	5.26
	Dehydroxylation stage	IV: 383.01–702.71	3.66
10	Dehydration stages	I: 44.88–140.82	3.77
		II: 140.82–207.09	5.32
		III: 207.29–387.28	5.52
	Dehydroxylation stage	IV: 387.28–706.7	3.94
15	Dehydration stages	I: 47.11–148.24	3.83
		II: 148.24–222.3	5.72
		III: 222.3–402.18	5.48
	Dehydroxylation stage	IV: 402.18–711.75	3.57
20	Dehydration stages	I: 50.59–153.1	3.93
		II: 153.1–230.8	5.89
		III: 230.8–407.6	4.98
	Dehydroxylation stage	IV: 407.6–717.55	3.86

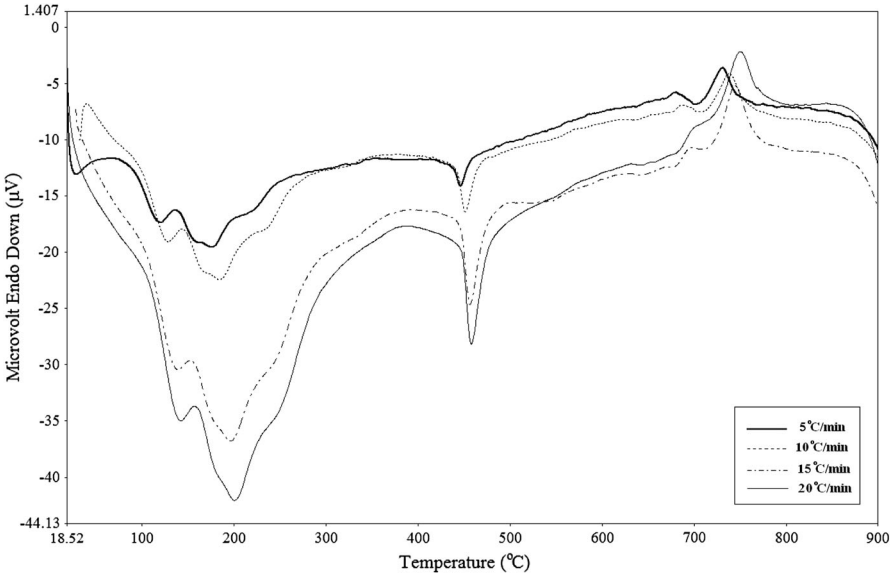

Fig. 6 DTA thermograms of tunellite at different heating rates

by using C–R, H–M, P–N, DY, and OW methods. In addition, by using C–R and H–M methods, the n value that gave the best fit was chosen as the order parameter for the dehydration steps of interest.

In the C–R method, n values are estimated until the best straight line is obtained for all stages. The correct n value thus estimated leads to the straight plots with maximum square correlation coefficient (R^2), from which the Ea is determined. The kinetic parameters computed using the C–R method are listed in Table 3. The Ea and k_0 values varied between 28.09 and 32.15 kJ/mol and 0.42×10^3–2.84×10^3 min^{-1} for stage I, 103.19–110.16 kJ/mol and 4.10×10^{11}–3.82×10^{12} min^{-1} for stage II, and 77.09–112.47 kJ/mol and 8.46×10^6–6.73×10^{10} min^{-1} for stage III, respectively.

In the H–M method, the best n values were found for first two stages because the n values for the third stage are greater than 4 ($n > 4$). Also, as seen in Table 3, the kinetic parameters computed with the H–M method are higher than the C–R and P–N equations. The reason of these situations was the inherent error involved in the approximation method employed in the derivation using the H–M equation. According to the H–M method, Ea and k_0 values varied between 40.68 and 44.97 kJ/mol and 3.23×10^4–4.04×10^5 min^{-1} for stage I and 124.03–130.97 kJ/mol and 1.21×10^{14}–1.18×10^{15} min^{-1} for stage II, respectively (Table 3).

In the P–N method, Ea and k_0 values varied between 28.10 and 32.16 kJ/mol and 0.34×10^4–1.44×10^4 min^{-1} for stage I, 53.08–58.52 kJ/mol and 8.46×10^4–2.28×10^5 min^{-1} for stage II, and 32.32–44.38 kJ/mol and 0.28×10^4–2.09×10^4 min^{-1} for stage III, respectively (Table 3).

Comparing the kinetic parameters computed by using the H–M, C–R, and P–N equations, it is observed that the values obtained from H–M are higher. This is due to the inherent error involved in the approximation method employed in the derivation of the H–M equation

In the DY method, E_a, k_0 and R^2 values were computed as 77.82 kJ/mol, 2.71×10^{12} min^{-1} and 0.9692 for stage I, 92.85 kJ/mol, 8.54×10^{12} min^{-1}, and 0.9562 for stage II, and 109.36 kJ/mol, 4.74×10^{13} min^{-1}, and 0.9986 for stage III, respectively (Table 3).

The OW method also gives the activation energy according to the degree of conversion. E_a values were calculated in the α range of 0.1–0.9 with an increment of 0.1 for all stages. E_a and R^2 for each α values at different stages are listed in Table 4. R^2 varied between 0.9589 and 0.9987 at different α values (0.1–0.9), and E_a values varied from 86.85 to 105.64 kJ/mol for stage I, 0.8813–0.9414 and 83.34–98.22 kJ/mol for stage II, and 0.7,380–0.8,984 and 86.97–151.60 kJ/mol for stage III, respectively.

Despite the differences between the E_a values calculated from using the C–R, H–M, and P–N equations, the OW and DY methods gave very similar values for the activation energy. This is because the OW method uses Doyle's approximation for the integrated rate equation.

The calculated activation energies for all dehydration stages by using all kinetic methods varied due to the different conception of the C–R, H–M, P–N, DY, and OW methods. The above differences in the determined kinetic parameters can be expected, because for all the equations except OW were based on single heating rate methods and they involve a systematic error. However, the isoconversional OW method is based on multiple heating rate methods. The isoconversional method allows the attaining of the dependence of the kinetic parameters using the

Table 3 Kinetic parameters were determined using the C–R, H–M, P–N, and DY methods

Model	Stage	β (°C/min)	5	10	15	20
C–R	I	n	0	0	0	0
		k_0 (min^{-1})	0.422×10^3	2.844×10^3	1.344×10^3	1.799×10^3
		E_a (kJ/mol^{-1})	28.09	32.15	29.22	29.55
		R^2	0.9968	0.9986	0.9986	0.9981
	II	n	1.79	1.67	1.68	1.73
		k_0 (min^{-1})	3.22×10^{12}	3.82×10^{12}	4.39×10^{11}	4.10×10^{11}
		E_a (kJ/mol^{-1})	110.16	109.76	103.19	103.21
		R^2	0.9961	0.9958	0.9960	0.9963
	III	n	2.91	3.33	3.33	3.65
		k_0 (min^{-1})	8.46×10^6	1.18×10^9	4.06×10^9	6.73×10^{10}
		E_a (kJ/mol^{-1})	77.09	94.36	100.60	112.47
		R^2	0.9848	0.9867	0.9881	0.9893
H–M	I	T_s (K)	390.14	397.05	406.11	408.48
		n	0.16	0.27	0.29	0.31
		k_0 (min^{-1})	3.234×10^4	4.039×10^5	2.306×10^5	3.051×10^5
		E_a (kJ/mol^{-1})	40.68	46.80	44.59	4.97
		R^2	0.9986	0.9994	0.9990	0.9987
	II	T_s (K)	447.09	452.14	464.24	469.36
		n	2.05	1.91	1.94	2.01
		k_0 (min^{-1})	1.18×10^{15}	1.12×10^{15}	1.33×10^{14}	1.21×10^{14}
		E_a (kJ/mol^{-1})	130.97	130.04	124.03	124.21
		R^2	0.9963	0.9959	0.9962	0.9965

Table 3 continued

Model	Stage	β (°C/min)	5	10	15	20
P–N	I	k_0 (min^{-1})	0.340×10^4	1.245×10^4	1.072×10^4	1.440×10^4
		E_a (kJ/mol^{-1})	28.10	32.16	29.23	29.55
		R^2	0.9968	0.9986	0.9985	0.9981
	II	k_0 (min^{-1})	8.455×10^4	2.275×10^5	1.669×10^5	1.667×10^5
		E_a (kJ/mol^{-1})	55.70	58.52	54.55	53.08
		R^2	0.9300	0.9371	0.9363	0.9323
	III	k_0 (min^{-1})	0.361×10^4	0.278×10^4	1.164×10^4	2.094×10^4
		E_a (kJ/mol^{-1})	39.40	32.32	41.34	44.38
		R^2	0.8442	0.8052	0.8353	0.8414
DY	I	T_m (K)	393.3	401.57	412.18	415.35
	Ea (kJ/mol)	77.82	k_0 (min^{-1})	2.71×10^{12}	R^2	0.9692
	II	T_m (K)	449.91	457.32	466.36	74.47
	Ea (kJ/mol)	92.85	k_0 (min^{-1})	8.54×10^{12}	R^2	0.9562
	III	T_m (K)	494.54	507.48	515.42	520.00
	Ea (kJ/mol)	109.36	k_0 (min^{-1})	4.74×10^{13}	R^2	0.9986

Table 4 Activation energies and square correlation coefficient of each α values at different stages from OW Methods

α	E_{a1}	R_1^2	E_{a2}	R_2^2	E_{a3}	R_3^2
0.1	86.85	0.9589	98.22	0.9414	86.97	0.8850
0.2	95.13	0.9799	95.16	0.9387	92.32	0.8984
0.3	105.64	0.9987	93.17	0.9308	96.93	0.8859
0.4	106.61	0.9974	90.90	0.9272	103.61	0.8420
0.5	104.42	0.9931	89.42	0.9239	112.85	0.7698
0.6	103.72	0.9877	88.60	0.9177	124.83	0.7514
0.7	103.17	0.9824	85.66	0.9072	137.07	0.7479
0.8	104.03	0.9750	84.52	0.8961	140.00	0.7380
0.9	105.06	0.9672	83.34	0.8813	151.60	0.7837
Average	E_{a1}:101.63 kJ/mol		E_{a2}:89.89 kJ/mol		E_{a3}: 116.24 kJ/mol	

conversion information from TG and DTG curves, which were determined through the measurements at different heating rates without making any assumptions regarding the reaction function and the order of the reaction. The isoconversional method, together with other multi-heating rate methods, are the most reliable techniques to describe the kinetic analysis of thermal data, as reported in the ICTAC Kinetic Project [24, 25]. Thus, the calculated activation energies by the OW method are more reliable than those obtained from the other kinetic methods.

Conclusion

The following key remarks can be made from this study:

- The thermal decomposition of tunellite occurred in three dehydration stages followed by one dehydroxylation stage. Based on the results of this work, the dehydration and dehydroxylation reactions are proposed to take place according to the following mechanisms:
- Dehydration stage:

$$(1)\quad SrO \cdot 3B_2O_3 \cdot 4H_2O \xrightarrow{36-153\,^{\circ}C} SrO \cdot 3B_2O_3.3H_2O + \sim H2O$$

$$(2)\quad SrO \cdot 3B_2O_3 \cdot 3H_2O \xrightarrow{153-231\,^{\circ}C} SrO \cdot 3B_2O_3 \cdot 2H_2O + \sim H2O$$

$$(3)\quad SrO \cdot 3B_2O_3 \cdot 2H_2O \xrightarrow{231-408\,^{\circ}C} SrO \cdot 3B_2O_3 \cdot H_2O + \sim H2O$$

- Dehydroxylation stage: $SrO \cdot 3B_2O_3 \cdot H_2O \xrightarrow{408-718\,^{\circ}C} SrO \cdot 3B_2O_3 + \sim H2O$

In this study, the thermal dehydration kinetics of tunellite was investigated by means of TG/DTG/DTA techniques, and kinetic parameters were estimated by using the C–R, H–M, P–N, DY, and OW methods. For the first stage thermal dehydration, the values of E_a vary from 29.75 to 101.63 kJ/mol and for the second stage, the E_a values were calculated as 55.46–127.31 kJ/mol. In addition, the values of E_a for the third dehydration stage were computed as 39.36–116.24 kJ/mol. This

variation of the activation energy was confirmed by the application of the different conception of kinetic methods. It was found that activation energies obtained by the isoconversional OW method for all dehydration stages are more reliable since this method is based on multi-heating rate methods.

Acknowledgment We gratefully acknowledge that this study was supported by The Prime Ministry State Planning Organization (Project No: 23-DPT–07–01–02).

References

1. Eti, 2007 Year Annual Report Eti Mine Works General Management, Turkey, 2007
2. C. Helvacı, R.N. Alonso, Turkish. J. Earth Sci. **9**, 1 (2000)
3. O. Baysal, Bull. Mineral. Res. Expl. Ins. Turk. **79**, 22 (1972)
4. H. Gülensoy, T. Teberdar, Bull. Mineral. Res. Expl. Ins. Turk. **79**, 30 (1972)
5. B. Caifeng, A. Xiaokang, F. Yuhua, B. Shuangyu, X. Sitan, J. Chil. Chem. Soc. **4**, 1291 (2007)
6. J.W. Park, S.C. Oh, H.P. Lee, H.T. Kim, K.O. Yoo, Korean, J. Chem. Eng. **17**(5), 489 (2000)
7. M. Sari Yilmaz, S. Kasap, S. Piskin, J. Therm. Anal. Calorim. **112**, 1325–1333 (2013)
8. M. Sarı Yılmaz, Y. Kalpaklı, S. Pişkin, J.Therm. Anal. Calorim. 10.1007/s10973-013-3152-x, (2013)
9. S. Piskin, PhD Thesis, Istanbul Technical University, Metallurgy Dept., Istanbul, Turkey, 22 (1983)
10. A. Ekmekyapar, A. Baysal, A. Künkül, Ind. Eng. Chem. Res. **36**, 3487 (1997)
11. F. Sevim, F. Demir, M. Bilen, H. Okur, Korean, J. Chem. Eng. **23**(5), 736 (2006)
12. S. Şener, G. Özbayoğlu, Ş. Demirci, Thermochim. Acta. **362**, 107 (2000)
13. H. Okur, Ç. Eymir, Ind. Eng. Chem. Res. **42**, 3642 (2003)
14. Y. Erdogan, A. Zeybek, A. Sahin, A. Demirbas, Thermochim. Acta. **326**, 99 (1999)
15. A. Kantürk, M. Yilmaz Sari, S. Piskin, Mater. Charact. **6**(61), 640–647 (2010)
16. Derun Moroydor E., Kipcak S. A., Senberber F. T., Yilmaz Sari M., Res. Chem. Intermediat. doi 10.1007/s11164-013-1237-6, (2013)
17. A. Kantürk, M. Sarı, S. Pişkin, Korean J. Chem. Eng. **25**(6), 1331 (2008)
18. M. Yilmaz Sari, S. Piskin, J. Chem. Soc. Pakistan. **34**(3), 526–532 (2012)
19. H.H. Horowitz, G. Metzger, Anal. Chem. **35**, 1464 (1963)
20. K.K. Bamzai, S.S. Kumar, Mater. Chem. Phys. **107**, 200 (2008)
21. C.D. Doyle, J. Appl. Polym. Sci. **639**, 6 (1962)
22. T. Ozawa, B. Chem, Soc. Jpn. **38**, 1881 (1965)
23. A.W. Coats, J.P. Redfern, Nature. **68**, 201 (1964)
24. M.E. Brown, M. Maciejewski, S. Vyazovkin, R. Nomen, J. Sempere, A. Burnham, J. Opfermann, R. Strey, H.L. Anderson, A. Kemmler, R. Keuleers, J. Janssens, H.O. Desseyn, C.R. Li, T.B. Tang, B. Roduit, J. Malek, T. Mitsuhashi, Thermochim. Acta. **355**, 125 (2000)
25. S. Vyazovkin, A.K. Burnham, J.M. Criado, L.A. Pérez-Maqueda, C. Popescu, N. Sbirrazzuoli, Thermochim. Acta. **520**(1–2), 1–19 (2011)